

MECHANICAL PROPERTIES OF NANOSTRUCTURED MATERIALS

Bing Q. Han¹, Enrique J. Lavernia¹ and Farghalli A. Mohamed²

¹Department of Chemical Engineering and Materials Science, University of California, Davis, CA 95616-5294, USA

²Department of Chemical Engineering and Materials Science, University of California, Irvine, CA 92697-2575

Received: January 29, 2005

Abstract. In this paper, the mechanical properties of nanostructured materials, defined hereafter as having a mean grain size that falls in the 50-200 nm ranges, is reviewed and the underlying mechanisms are discussed. Particular emphasis is placed on nanostructured materials that are processed via two synthesis approaches: consolidation of nanocrystalline powders and electrodeposition. The present review demonstrates that processing history significantly influences mechanical behavior as revealed by the following observations. First, a low strain hardening behavior is usually observed during the plastic deformation of nanostructured materials processed by milling (also known as mechanical milling or attrition). The phenomenon can be attributed to the process of dislocation annihilation or dynamic recovery during plastic deformation. Second, the reported asymmetry of yield strength between tension and compression can be rationalized based on the existence of porosity or the presence of a bimodal phase distribution. Third, significant strain hardening behavior is generally observed in nanostructured materials processed by electrodeposition. The observation of strain hardening in nanostructured materials can be explained on the basis of dislocation multiplication. Fourth, the low ductility that is frequently reported for nanostructured materials is related to an absence of dislocation activity. Recent work reviewed suggests that this limitation may be surmounted by implementing the concept of multiple length scales in the microstructure.

1. INTRODUCTION

Nanostructured materials reportedly exhibit unique microstructures and enhanced mechanical performance [1,2]. As a result, they have attracted considerable attention in recent years and offer interesting possibilities related to many structural applications. Although nanostructured materials are traditionally defined as those with grain sizes that are smaller than 100 nm, grains in excess of 100 nm are typically present in the microstructure primarily as a result of the broad distribution of grain sizes that evolves during processing. Therefore, we heretofore define nanostructured materials as those

with grain sizes smaller than 200 nm and with an average grain size of less than 100 nm.

The successful synthesis of large-scale nanostructured materials with grain sizes in the range of 10 – 200 nm represents a major achievement in the emerging field of nanotechnology [3]. Inspection of the scientific literature indicates that there are many techniques that can be used to produce nanostructured materials, including inert gas condensation or chemical vapor condensation [1,4], pulse electron deposition [5], plasma synthesis [6], crystallization of amorphous solids [7], severe plastic deformation [8], and consolidation of mechanically alloyed or cryomilled powders [9,10]. However,

Corresponding author: Farghalli A. Mohamed, e-mail: famohame@uci.edu

only a few of these techniques, such as electro-deposition [5,11] and consolidation of mechanically alloyed/cryomilled powders [9,10], generate nanostructures with sufficient thermal stability to permit the fabrication of bulk materials.

The present review will specifically address the mechanical properties, primarily room temperature tensile and compressive behavior, of nanostructured materials, since the topic of creep and superplastic behavior of nanostructured materials has been comprehensively presented in an earlier review [12]. The purpose of the present study is two-fold: (a) to review current experimental data reported for mechanical performance of nanostructured materials, and (b) to discuss the deformation mechanisms of nanostructured materials.

2. MECHANICAL PERFORMANCE OF NANOSTRUCTURED MATERIALS

2.1. Mechanical properties of nanostructured materials processed by consolidation of nanostructured powders

Inert-gas condensation. Nanocrystalline materials can be manufactured by the consolidation of powders from inert-gas condensation techniques [4,13,14]. For instance, nanocrystalline Cu and Pd alloys with grain sizes of 10 - 22 nm and 16 - 54 nm, respectively, were made by compaction of powders from an improved technique of inert-gas condensation, with a density of 98-99% in the nanostructured Cu and Pd alloys [15], which is much higher than that (97 - 72%) reported in a previous study [16]. Tensile tests of nanocrystalline Cu and Pd alloys were investigated [15]. Inspection of tensile results of the nanocrystalline Cu reveals that the tensile behavior of the nanostructured Cu and Pd alloys is significantly influenced by the residual porosity after compaction and values of Young's modulus of the nanostructured Cu and Pd alloys increases with decreasing fraction of porosity. Because of the existence of porosity, all the nanostructured specimens failed in the strain-hardening region. The residual porosity also has an influence on the compression behavior of nanostructured Cu and Pd alloys [17]. For example, nanostructured Cu and Pd alloys with a low density (92.5% and 95.3% theoretical density, respectively) also exhibit a low strength (compressive yield strength of 650 MPa and 750 MPa, respectively). A prolonged compressive plastic deformation as well as apparent strain hardening ability is observed in

the nanostructured Cu and Pd alloys (compressive yield strength of 850 MPa and 1100 -1130 MPa, respectively) with a higher density (~98%). In addition, it is noteworthy that the reported tensile yield strength is lower than the corresponding compressive value. Hence, the asymmetry of yield strength in nanostructured Cu and Pd alloys can be attributed to the presence of residual porosity and incomplete bonding during compaction [17]. Therefore, eliminating the porosity in nanostructured materials processed via inert-gas condensation and condensation is a critical challenge for the improvement of tensile properties.

In other related studies, the mechanical properties of nanocrystalline Al-Zr alloys processed by compaction of inert-gas condensation were investigated [18]. There is only a short elongation of 0.3% in the specimen of a nanocrystalline Al-6.4%Zr alloy with grain sizes of ~10 nm. In contrast, a high elongation of ~ 2.5%, as well as significant strain hardening behavior were noted during tensile deformation of a bimodal nanocrystalline Al-0.6%Zr alloy. This apparent discrepancy was attributed to the heterogeneous distribution of solute in the microstructure, which effectively led to the formation of a bimodal distribution of grain sizes: some parts of the specimen was nanocrystalline, while other regions contains grains that were > 100 nm in size [18]. High ductility and strain hardening behavior were attributed to the dislocation activity in the larger grained regions.

Ball milling. Ball milling is a widely used approach for the preparation of nanostructured powders. During milling, the materials experience severe plastic deformation, resulting in grain refinement. As indicated by Fecht [19], grain size in powders decreases with increasing milling time and ultimately reaches a saturated minimum grain size. The minimum grain size obtainable by milling has been attributed to a balance between the grain refinement introduced by severe impact deformation of milling and its thermal recovery due to the material itself [19-21]. These studies have led to following important observations and findings: (1) grain size obtainable in milling decreases with increasing milling time, reaching a minimum grain size, that is characterized by each metal, (2) the minimum grain size scales inversely with the melting point or the bulk modulus of each metal, (3) there is a linear relationship between the minimum grain size and the critical equilibrium distance between two edge dislocations in FCC metals, and (4) limited experimental evidence suggests

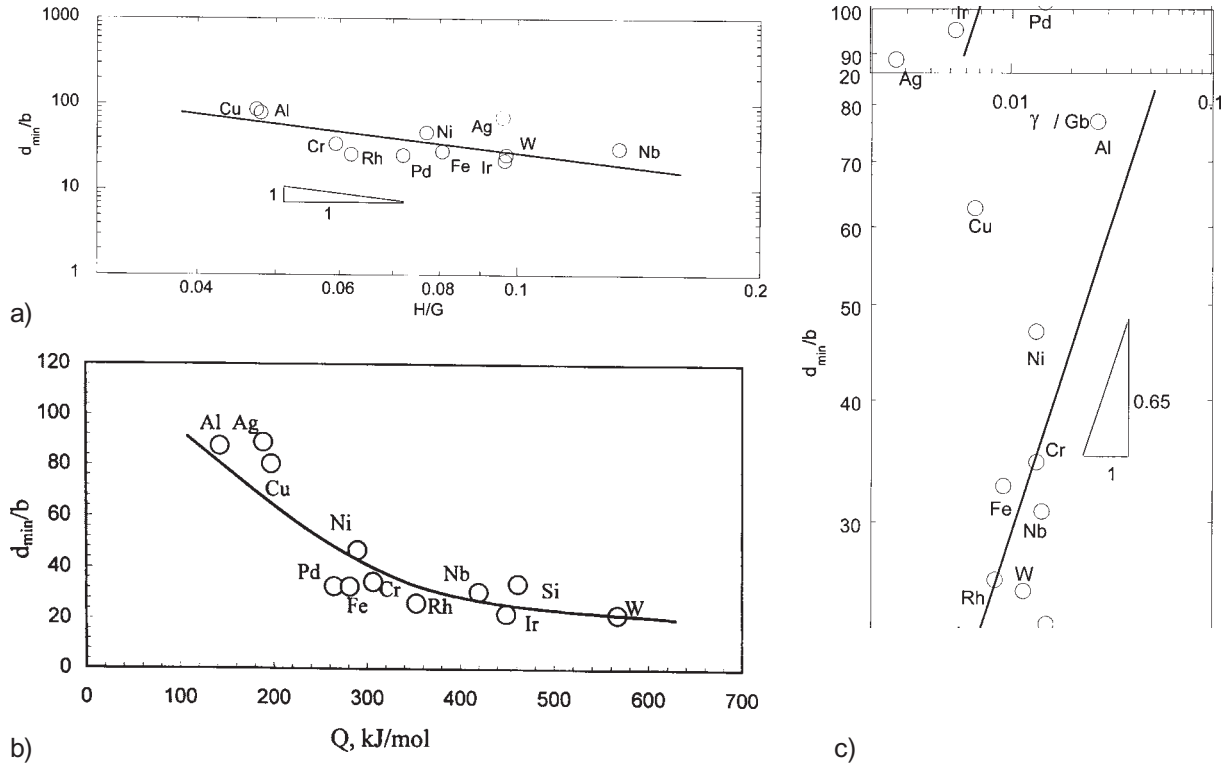


Fig. 1. (a) Normalized minimum grain size, d_{min}/b , obtained by milling as a function of the normalized hardness, H/G , (logarithmic scale); (b) Normalized minimum grain size, d_{min}/b obtained by milling as a function of Q ; and (c) Normalized minimum grain size, d_{min}/b obtained by milling as a function of the normalized stacking fault energy, γ/Gb , (logarithmic scale) [22].

that smaller grain sizes are achieved at lower milling temperatures.

Most recently, Mohamed developed a dislocation modeling to quantitatively describe the minimum grain size obtainable in milling [22]. According to this model, the minimum grain size is governed by a balance between the hardening rate introduced by dislocation generation and the recovery rate arising from dislocation annihilation and recombination. By balancing the rate of grain size decrease and the rate of grain size increase, the minimum grain size (d_{mini}) is given by [22]

$$\frac{d_{min}}{b} = A_3 \exp\left(-\frac{\beta Q}{4RT}\right) \left(\frac{D_{PO} G b^2}{v_0 k T}\right)^{0.25} \left(\frac{\gamma}{Gb}\right)^{0.5} \left(\frac{G}{\sigma}\right)^{1.25}, \quad (1)$$

where b is the value of Burgers vector, A_3 is a dimensionless constant, β is constant, Q is the self-diffusion activation energy, R is the gas constant, T is the absolute temperature, D_{PO} is the diffusion coefficient, G is the shear modulus, v_0 is the initial

dislocation velocity, k is Boltzmann's constant, γ is the stacking fault energy and σ is the applied stress. The model predicts that the minimum grain size depends on hardness, stacking fault energy for recovery, and an exponential function of the activation energy for recovery.

These predictions quantitatively agree reasonably well with experimental results and trends as demonstrated by Fig. 1. The data of normalized minimum grain size, d_{min}/b , obtained by milling for FCC metals (Al, Cu, Ni, Pb, Rh, and Ir), as a function of the normalized hardness, H/G , show an inverse trend on a logarithmic scale, fitting very well with predictions, as shown in Fig.1a. The data of normalized minimum grain size, d_{min}/b for both FCC metals and BCC metals, are plotted as a function of the Q , showing an exponentially decreasing trend, which is consistent with the theory prediction in Fig.1b. The data of normalized minimum grain size, d_{min}/b on FCC and BCC metals as a function of the normalized stacking fault energy, γ/Gb , on a logarithmic scale are shown in Fig.1c. The data points for all metals, with the exception of Ag, fit a straight line as predicted by the theory [22].

After consolidation under appropriate conditions, bulk nanostructured materials can be obtained from nanostructured powders. There are several popular approaches for consolidation: high-temperature sintering, hot isostatic pressing (HIP) at elevated temperatures or cold isostatic pressing (CIP) at ambient temperatures, in which HIP is a more effective means for generating high density bulk. Following consolidation, secondary processing is sometimes performed to remove any remaining porosity of the consolidated billets and improve mechanical properties since the consolidated materials usually have a density lower than the theoretical density. Several examples of mechanical properties of nanostructured materials prepared by milling are analyzed herein.

Nanostructured Fe-10Cu alloys were prepared by ball milling, followed by HIP and forging at different conditions [23]. Grain size values in the range of 30 nm to 1.7 μm were obtained. Shear fracture immediately following yielding was observed in compression of nanostructured Fe-10Cu alloy with grain sizes less than 150 nm. In comparison, elastic-perfectly plastic deformation and finally shear bands were observed in compression of nanostructured Fe-10Cu alloy with grain sizes larger than 300 nm. The compressive yield strength of the Fe-Cu alloy was reported to be approximately 30 pct higher than the tensile yield strength. The tension-compression asymmetry of the yield strength observed in the study was attributed to the effect of hydrostatic pressure dependence or a normal stress dependence (Mohr-Coulomb) of the yield criterion [23].

In other studies, nanocrystalline Al was prepared by means of sintering of nanocrystalline Al powders with a grain size of 53 nm by the active H_2 plasma evaporation method [9]. A low strain-hardening region (work softening) after yielding was observed in the tensile deformation of the bulk nanocrystalline Al. In addition, both ductility of the nanocrystalline Al increases and the stress drop behavior are improved after further cold deformation. Although there is no reasonable explanation on the deformation mechanisms of nanostructured Al, it appears that the secondary processing, cold deformation after sintering, has contributed to the elimination of processing residual defects, which have a significant influence on the low strain hardening behavior.

A high value of compression strength of 692 MPa is observed in nanocrystalline Al-5at.%Ti alloy with grain sizes of 50 – 100 nm, which is consolidated by plasma activated sintering from reactive ball milling [24]. However, the material is rather brittle and

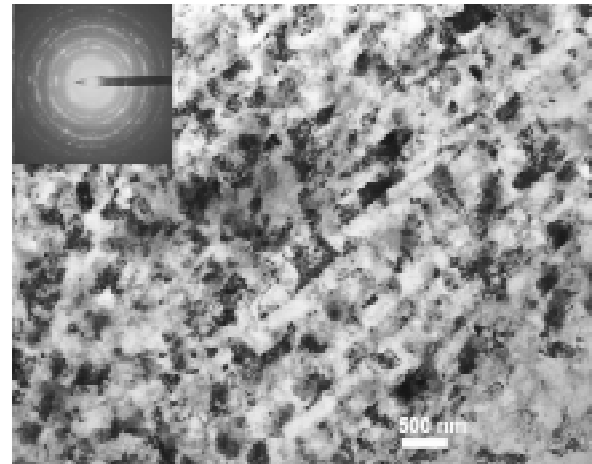
there is only about 5% plastic strain at the compression condition. Similar behavior is also observed in nanostructured V with grain sizes of ~ 100 nm, which was prepared by consolidation of mechanically alloyed powders [25]. Compression strength of higher than 2000 MPa was observed. A stress softening behavior was observed and the materials failed at a low strain level of 5%.

Near-perfect elastoplasticity, with a ductility of approximately 12 pct and without apparent necking, is observed in tensile deformation of nanocrystalline pure Cu processed via sintering of nanocrystalline powders [26]. Transmission electron microscope observation indicates that the nanostructured Cu produced is composed of grains with sizes of 50 – 80 nm, arranged in agglomerates with sizes between 200 and 300 nm. Because there are no strain hardening and necking, the phenomenon is difficult to explain using Considere criterion, which predicts plastic instability at $d\sigma/d\varepsilon \leq \sigma$ when necking should have occurred soon after yielding. The phenomenon is different from the low strain hardening behavior observed in ultrafine-grained Ti and Fe, which are prone to plastic instability [27,28].

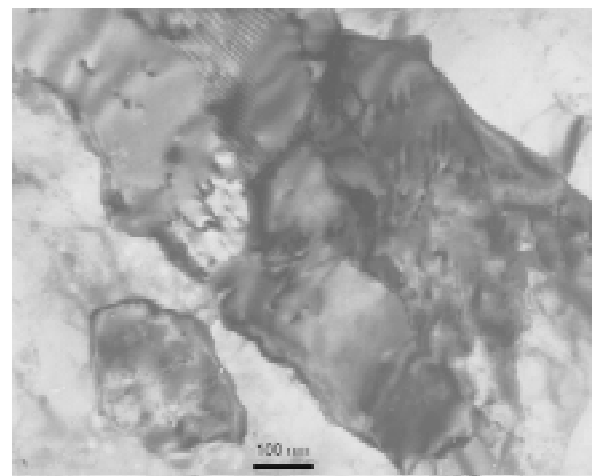
Cryomilling. Cryomilling has been developed into an effective means for manufacturing bulk nanostructured Al alloys in recent years. The processing of nanostructured Al alloys via cryomilling technique usually includes several steps [10,29]. The first step is cryomilling, i.e., the spray-atomized Al alloy powders are mechanically milled using stainless steel balls in a liquid nitrogen slurry. During cryomilling, ~ 0.2 wt.% of stearic acid is typically added into the powders to prevent the powder welding on the milling media. The cryomilled powder normally reveals a grain size of ~ 20 nm, as determined by X-ray diffraction (XRD) patterns and microstructure observed by TEM [30,31]. The second step is degassing. The milled powders are packed in Al cans in an inert gas atmosphere, followed by vacuum degassing at elevated temperatures to evaporate any organic phases in the powders (e.g., stearic acid). The third step is consolidation. The canned powders are then consolidated via hot isostatic pressing (HIP) at elevated temperatures or cold isostatic pressing (CIP) at ambient temperatures. The final step is secondary processing. Since the consolidated materials usually have a density lower than the theoretical density, a secondary processing at high temperatures, for instance, extrusion or forging, has to be performed to remove any remaining porosity of the consolidated billets and improve mechanical properties.

The microstructure of a nanostructured Al-Mg alloy after consolidation and extrusion [32] is shown in Fig. 2a. In the longitudinal direction, inspection of large areas parallel to the extrusion direction (Fig. 2a) reveals a homogeneous microstructure comprised of equiaxed grains, in which, however, the extrusion direction is evident from the preferred orientation of grains. Continuous rings of selected area electron patterns (SAED) indicate that the grains are separated by high-angle grain boundaries. The presence of five primary rings in the diffraction ring patterns is consistent with the lattice structure of aluminum matrix. The existence of dispersoids in the microstructure is not discernable from the diffraction ring patterns. This observation is most likely due to the extremely low volume fraction of dispersoids. The average grain size obtained based on individual measurement of 70 grains is approximately 120 nm. Dislocations are observed in some grains but were absent in others. There are a few small particles, with a size from 5 to 10 nm, expected to be dispersoids, in the bright field images with higher magnifications, as shown in Fig. 2b. The equiaxed grains without a preferred orientation of grains were observed in the microstructure viewed normal to the extrusion direction, as shown in Fig. 2c. The average grain size on the basis of 20 grains is approximately 90 nm.

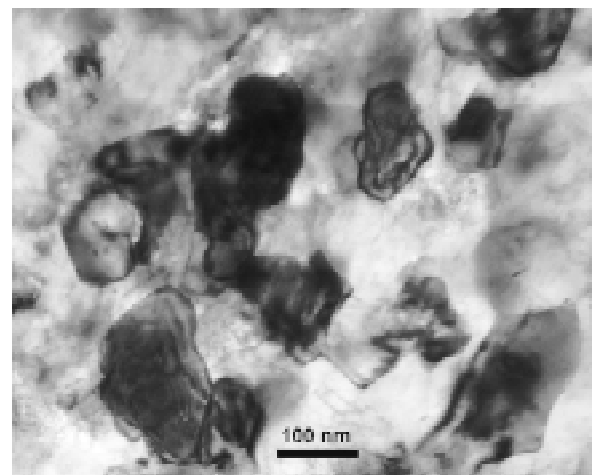
The tensile behavior of several Al-Mg alloys, i.e., a cryomilled nanostructured Al-7.5%Mg-0.3%Sc alloy [29], bimodal cryomilled Al-7.5%Mg alloys [33], a cryomilled UFG Al-7.5%Mg alloy [34], and a coarse-grained Al-6.64%Mg alloy [35], is shown in Fig. 3a. The cryomilled Al-Mg-Sc alloy and Al-Mg alloy have a grain size of about 200 nm and 300 nm, respectively. The near-nanostructured Al-Mg-Sc alloy exhibits a yield strength of 630 MPa, an ultimate tensile strength (UTS) of 730 MPa, and an elongation-to-failure of approximately 2.7 pct. Although the material consolidated from fully cryomilled nanostructured Al-Mg powders has a high strength (yield strength of 642 MPa and UTS of 847 MPa), it fails in the strain-hardening region, resulting in a low ductility (only 1.4%). Inspection of the curves reveals a brief strain-hardening region from yielding to the maximum stress and a low strain-hardening region. The strain hardening exponent, n ($n = d \ln \sigma / d \ln \epsilon$), is very low or negative in the cryomilled Al-7.5Mg alloy, whereas, the strain-hardening exponent is relatively high (about 0.36) in the coarse-grained Al-Mg alloy. In addition to the presence of low strain hardening behavior, the localized shear bands (Lüders band) and a macroscopic neck-



a)



b)



c)

Fig. 2. Microstructure of an extruded nanostructured Al-Mg alloy in (a) (b) longitudinal and (c) transverse directions [32].

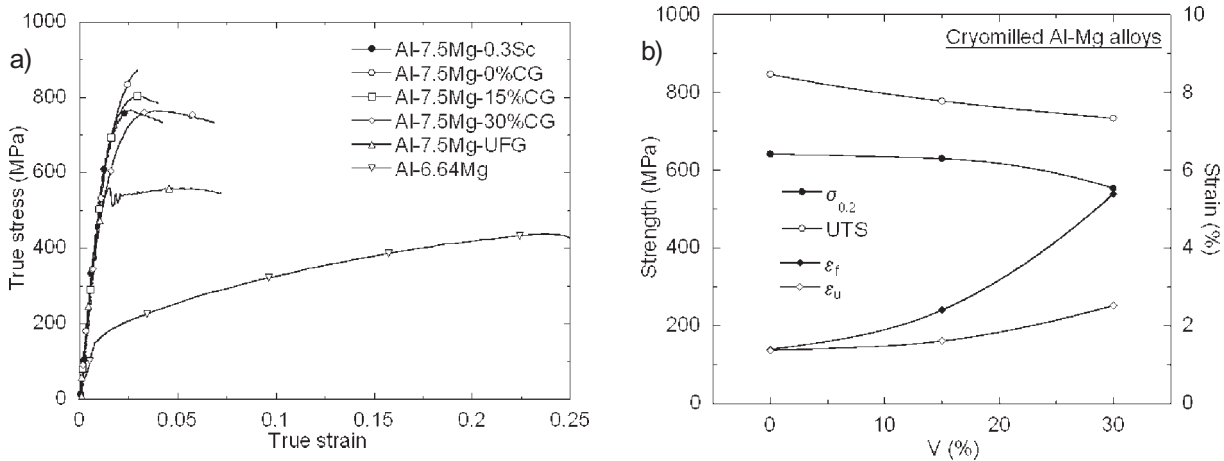


Fig. 3. (a) Tensile behavior of cryomilled Al-Mg-Sc [29], bimodal cryomilled Al-Mg alloys [33] and cryomilled UFG Al-Mg alloy [34] compared to an Al-Mg alloy [35]. (b) The effect of volume fraction of unmilled submicron-grained materials on strength and ductility of bimodal cryomilled Al-Mg alloys [33,36].

ing, especially in the plate thickness direction, were observed.

Inspection of published results reveals that in some cases, bimodal Al-Mg alloys [33] have higher strength but lower ductility than those of similar ultrafine-grained Al-7.5%Mg alloy [34] and conventional Al-Mg [34]. Moreover, there is a trend of decreasing strength and increasing elongation with increasing fraction of submicron-grained regions occurs, as shown in Fig. 3b [33,36]. The nanostructured regions of bimodal Al-7.5%Mg alloy have grain sizes of 100 – 300 nm and submicron-grained bands have a grain size of $\sim 1 \mu\text{m}$ [33]. The optical microstructure of an extruded cryomilled Al-Mg alloy containing 30% unmilled submicron grains is shown in Figs. 4a and 4b. The dark areas are cryomilled nanostructured regions and the grayscale regions are the unmilled submicron-grained regions, which are distributed along the extrusion direction. A good combination of strength and ductility is obtained in the cryomilled Al-Mg alloy with 30% of submicron-grained regions.

In an effort to enhance our understanding of the mechanisms that are responsible for the behavior of bimodal materials, a number of numerical studies have been published [37,38]. A two-dimensional, self-consistent embedded unit-cell model, which is based on fundamental continuum mechanics at the meso-scale and extracted from a random array of particles in the case of a composite material, provides an ideal approach that is used to simulate the stress distribution and deformation behavior in metal matrix composites [37,38]. In one example, the unit-

cell model was employed to model the uni-axial tensile behavior during elastic-plastic deformation of bimodal nanostructured Al-Mg alloys [36]. It is observed that the meshes still remain intact when the applied stress reaches the yield strength, and, in addition, that the stress/strain distribution remains uniform immediately after yielding since there is no distortion in any domain. With the onset of plastic deformation, the stress field becomes heterogeneous and the plastic strain tends to be concentrated in the vicinity of interfaces at the lateral sides of submicron grains. Von Mises stress distribution for the Al-Mg alloy with 30% submicron grains after fracture initiation is shown in Fig. 4c. It is observed that the stress heterogeneity is even worse after the failure of elements, resulting in higher stress in the lateral areas than that in the axial direction [36]. The fracture surface of the bimodal Al-Mg alloy with 30 pct submicron grains is shown in Fig. 4d. Delamination at interfacial areas between nanostructured regions and submicron-grained regions occurs in both cases, indicating large deformation occurs at interfaces during nucleation and propagation of cracks. The necking deformation and the dimple morphology are also observed in the submicron-grained regions, which indicate that there is significant plastic deformation in the submicron-grained regions via a ductile bridging mechanism [36].

In related studies, the tensile behavior of nanostructured Al-10Ti-2Cu alloy, processed via cryomilling technique, was reported [39,40]. Examination of many representative micrographs indicated that the microstructure of the nanostructured Al-10Ti-

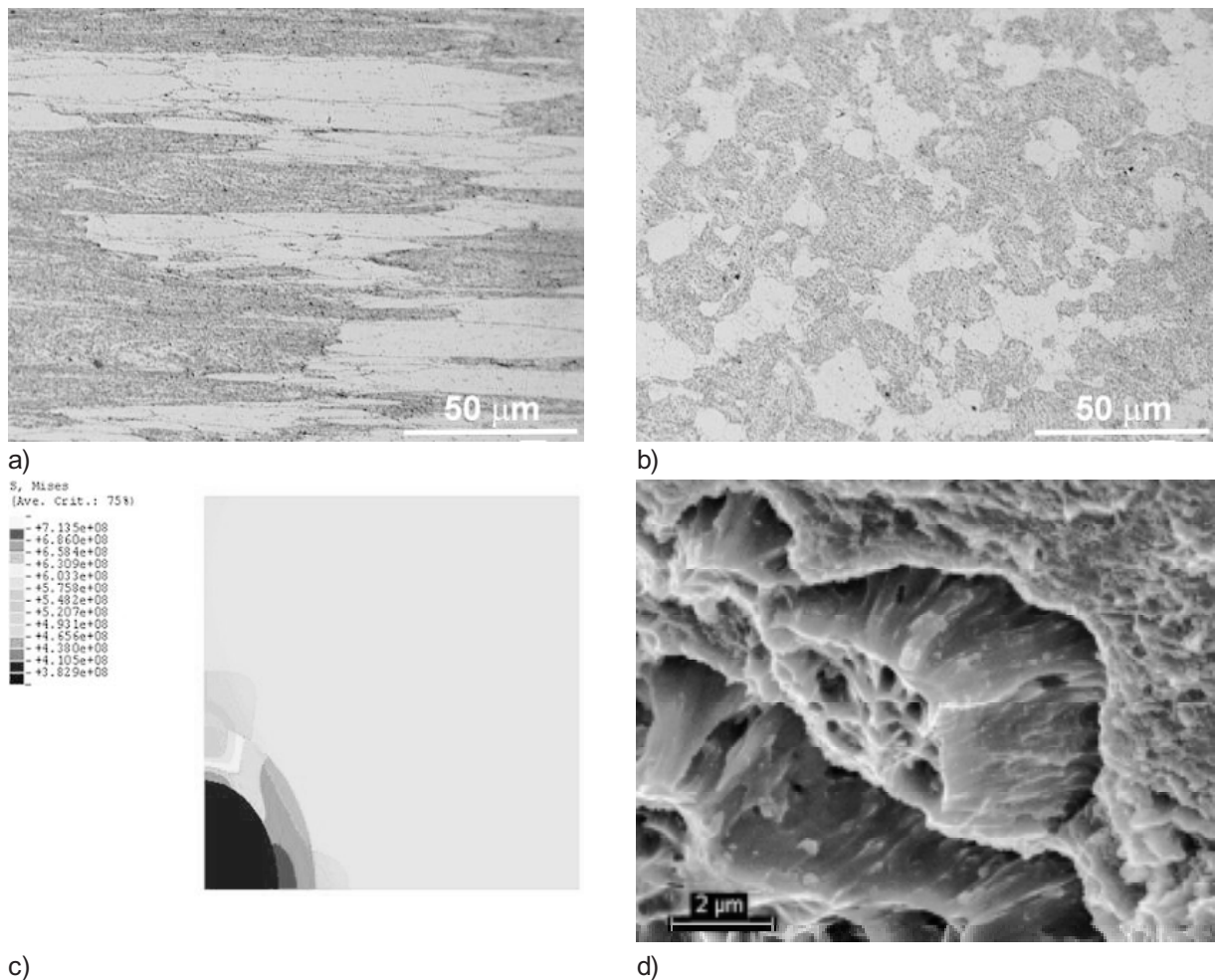


Fig. 4. Optical microstructure of cryomilled Al-Mg alloy containing 30% submicron-grained regions in (a) longitudinal and (b) transverse directions. (c) Von Mises stress distribution for the Al-Mg alloy with 30% submicron grains after fracture initiation [36]. (d) Fractography of the bimodal Al-Mg alloys with 30% submicron grains.

2Cu alloy consists of two phases, approximately 90% nanostructured regions containing grains of 30–70 nm and 10% coarse-grained phase around boundaries of the former regions, which appear as ‘islands’ in the matrix of the nanostructured phase, are distributed along the extrusion direction with a width of about 2 mm. Compression behavior of the as-extruded Al-10Ti-2Cu alloy is compared with its tensile behavior in Fig. 5 [41]. Inspection of the figure reveals that there are a strain softening behavior in the compression of the nanostructured Al-10Ti-2Cu alloy and a small asymmetry of yield strength between tension and compression, with an ultimate strength ratio of 0.90–0.92. The asymmetry behavior of the nanostructured Al-Ti-Cu alloy was attributed to the presence of two spatial domains in the

microstructure rather than the intrinsic behavior of the nanostructured Al-Ti-Cu alloy [41].

In summary, ductility of nanostructured materials processed via milling decreased with decreasing grain size. The plastic deformation of nanostructured materials is characterized by a short region of strain hardening, followed by a region of low strain hardening or work softening behavior. Although dislocation movement is expected because of relatively large grain size (50 – 200 nm), strain-hardening region is very short, resulting in the value of yield strength very close to that of ultimate tensile strength. Ductility in the nanostructured materials with bimodal microstructure is increased, as manifested with a longer low strain hardening or work softening region.

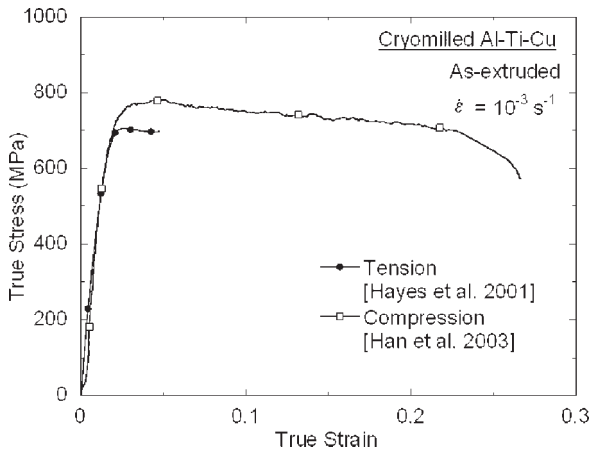


Fig. 5. The tension-compression asymmetry of nanostructured Al-Ti-Cu alloy [41].

2.2. Mechanical properties of nanostructured materials processed by electrodeposition

Electrodeposition is an effective approach to manufacture sheets of nanocrystalline materials, such as sheets of Ni, Cu and several other nanocrystalline metals with grain sizes of 10 – 40 nm and a thickness of 100 – 300 μm [11,42]. The success of electrodeposited nanocrystalline materials with grains in the range of several nanometers makes it possible to investigate mechanical properties of materials in the nano-scale range, such as the validation of negative Hall-Petch relationship and the transition of deformation mechanisms from dislocation plasticity to grain boundary sliding (GBS).

Nanocrystalline Ni. A nanocrystalline Ni with grain sizes of 40 – 50 nm was prepared by a pulse electrodeposition technique and inspection of tensile tests reveals that there is a significant strain hardening region from yielding to the ultimate tensile strength with a tensile ductility of 1 – 3 pct [11]. Inspection of the strength results indicates that the Hall-Petch relationship is maintained well up to approximately 10 nm grain size. Therefore, the strain hardening is attributable to the accumulation of dislocations and eventually formation of dislocation cells. A strong temperature dependence of strength in nanocrystalline Ni is observed. The ratio of strength obtained at – 196 °C to strength obtained at room temperature in nanocrystalline Ni is much higher than that in coarse-grained Ni. Multiple deformation mechanisms are suggested to operate in nanocrystalline Ni and the high activation energy

deformation mechanism is suggested to be dislocation transmission through grain boundaries. However, because the grain size was characterized by X-ray diffraction techniques, the grain size distribution, grain boundary misorientation and the dislocation variation during plastic deformation were not reported. Therefore, there is no available experimental evidence that can support their explanation regarding the deformation mechanisms.

Similar tensile ductility of 2 – 4 pct and significant strain hardening behavior are observed in another nanocrystalline Ni with a grain size of 30 nm, which is prepared by a pulse electrodeposition technique [43]. In this study, grain boundary migration is proposed to be the dominant deformation mechanism at room temperature [43]. However, it is difficult to rationalize the observation of significant strain hardening behavior on the basis of the deformation mechanisms involving grain boundary migration.

In another report, tensile behavior of nanocrystalline electrodeposited Ni with grain sizes of ~ 20 nm was investigated at a wide range of strain rates from 10^{-5} to 10^3 s^{-1} [44]. In the low strain rate regime (10^{-5} to 10^{-2} s^{-1}), the maximal strains that can be obtained decrease from 2.2% to 0.4% with increasing strain rate, while the ultimate tensile strength remains almost approximately constant. In the high strain rate regime (10^0 to 10^3 s^{-1}), the ultimate tensile strength increase significantly with increasing strain rate, while the maximal strains range between 1.2 and 1.8%. The tensile ductility obtained in electrodeposited nanocrystalline Ni is usually less than 3%. The low ductility is argued to be attributable to the possible grain boundary contamination by impurity, especially sulfur, and/or the presence of cavities or pores along grain boundaries and probably also inside some grains [44]. Together with the pronounced increase in the UTS at high strain rates, a change in fracture characteristics is observed, as represented by the fracture surface at 55 - 65° corresponding to the angle of maximal shear under plain strain condition and the appearance of necking.

Recently, the influence of annealing and impurities on tensile properties of electrodeposited nanocrystalline Ni was investigated in detail [45]. The as-deposited Ni has grain sizes in the range of 5 – 50 nm and an average grain size of 29 nm. Annealing at 373K for 1 hour has a slight influence on the grain size. Abnormal grain growth was observed after annealing at 473K for 1 hour, generating the microstructure with a bimodal distribution of grain sizes, average grain size of 70 nm and 300 nm. Further annealing at 573K caused the growth of

most grains to the range of 1 – 2 μm . It is interesting to note that annealing treatment at temperatures of 373 and 423K enhanced tensile strength. This observation is rationalized in terms of relaxation of the non-equilibrium grain boundaries after annealing, resulting in more resistant of grain boundaries to dislocation activity [46]. Tensile strength decreased, as expected, after annealing at temperatures of higher than 473K. Tensile ductility only increased slightly after annealing at a temperature of 373K, and then decreased with increasing annealing temperature. It is interesting to note that although grain size is small in the as-deposited nanocrystalline Ni and the nanocrystalline Ni after annealing at 373K, there is a significant strain hardening behavior. The strain hardening behavior became apparent after annealing at temperatures of 423K and 473K due to the existence of submicron grains. There is almost no ductility in Ni after annealing at temperatures higher than 523K. Both strength and ductility decrease after annealing at the higher temperatures was attributed to the segregation of impurity sulfur along the grain boundaries [45].

The temperature dependence of strength of the electrodeposited Ni and Co alloys was investigated by comparing tensile strength at room temperature and at cryogenic temperature [47]. Very low value of activation volume ($\sim 10 b^3$) is observed in nc Ni and nc Co, compared to that ($800 - 1000 b^3$) in the coarse-grained Ni and Co. Therefore, the thermal activated deformation mechanism in nc materials might be different from that in the coarse-grained materials. It was argued that the forest spacing of dislocations in the nc Ni might be a couple of nanometers because of the small activation volume, excluding the accumulation of dense dislocations in the grain interior. Dislocations are emitted from grain boundary sources and travel through the grain to be incorporated into the opposing grain boundary, resulting in a rather small activation energy [47].

A nanocrystalline Ni-W alloy with a grain size of 8.1 nm was prepared by direct current electrodeposition [48]. Although there is a low value of elongation to failure (<1%), a dimple pattern of the fracture surface is observed. The microstructure of the nanocrystalline Ni-W alloy after tensile deformation is observed by high resolution electron microscopy. The observation of microstructure at the immediate vicinity of fractured surface reveals that there are many nano-sized grains with various contrasts. Both stacking faults and twins are observed in a few grains. It is interesting to note that there is a long wide curved band of linear defects along grain boundaries. Inspection of structural defects described above

suggests that grain boundary sliding might be the dominant deformation mechanism. In this case, each grain boundary undergoes different degree of sliding. A group of neighboring nanograins, rather than individual grain, slides together as grain clusters, as reflected by the dimple morphology [48].

Nanocomposites consisting of submicron size SiC particulates ($\sim 0.4 \mu\text{m}$) in a nanocrystalline Ni matrix with grain sizes as small as 10 nm were manufactured by the technique of pulse electrodeposition [49]. It is interesting to note that not only the tensile strength but also ductility of the nanocomposites with low SiC content (<2%) is higher than those of nanocrystalline Ni with the same grain size. The ductility of 3.4% was observed in the nanocomposite Ni with 0.7% SiC. However, at higher SiC content (>2%), the strength and ductility of the nanocomposites were found to be worse due to the particle clustering in the microstructure.

Nanocrystalline Cu and Co. The mechanical properties of electrodeposited nanocrystalline Cu have been recently reported. In this study, the nanostructured Cu processed by means of the electrodeposition technique has a grain size of ~ 28 nm, however, further observation by means of high resolution electron microscopy indicates that the as-deposited sample consists of ultrafine crystallites with sizes ranging from a few nanometers to about 80 nm, separated by low angle grain boundaries (with a misorientation of $1 - 10^\circ$) that comprised of dislocation arrays [50,51]. High values of strain to failure (15% - 55%) along with an obvious strain hardening behavior are observed in tensile behavior of the nanostructured Cu at strain rates of $6 \cdot 10^{-5} \text{ s}^{-1}$ to $1.8 \cdot 10^3 \text{ s}^{-1}$. Yield strength and ultimate tensile strength as well as ductility increase with increasing strain rate. It is interesting to note that although the grain sizes of the nanostructured Cu are much smaller than the corresponding coarse grained Cu, the value of flow stress in the former is much less than that in the latter. Superplastic extensibility during cold rolling is also observed in a nanostructured Cu prepared by electrodeposition [52]. A deformation mechanism dominated by grain boundary deformation, rather than by dislocation activity in the lattice was considered to be dominant.

The tensile behavior of nanocrystalline electrodeposited Co with an average grain size of 12 nm was investigated [53]. Not only flow strength, but also ductility increased with increasing strain rate during the tensile deformation. Elongation to failure of 9% is obtained at a strain rate of 10^{-4} s^{-1} . A smaller

work hardening exponent in nanocrystalline Co than in nanocrystalline Ni with a similar grain size is observed. The experimental observation in this study is different from the findings in electrodeposited nanocrystalline Ni with a similar grain size, which are usually explained by the dislocation slip behavior. On the basis of the observation of high concentration of stacking faults/microtwins in the microstructure, it was proposed that mechanical twinning plays an important role in the plastic deformation of nanocrystalline Co [53]. Twinning requires a higher activation stress than dislocation slip but then proceeds with relatively smaller stress increments, resulting in a lower work hardening exponent [53].

In summary, results of above several examples of electrodeposited nanocrystalline materials indicate that there is a significant strain hardening region after yielding before reaching the ultimate tensile strength and a region of low strain hardening or work softening after the maximum strength is not observed. It is interesting to note that although the grain size (~30 nm) in nanocrystalline materials processed by electrodeposition is rather smaller than that by milling, a significant strain hardening region is widely reported.

Nanostructured Al-Fe alloys. There are several bulk nanostructured materials processed using approaches, other than consolidation of milled powders or electrodeposition. For instance, bulk nanostructured Al-Fe alloys can be prepared by electron-beam deposition [54] when the atom fraction of Fe is higher than 2 pct. The tensile strength of deposited Al-Fe alloys increases with increasing Fe content, reaching 1000 MPa at 2.5 at.% Fe fraction. However, the ductility of deposited Al-Fe alloy decreases with increasing Fe content and is brittle at atomic fractions higher than 2.5. A good combination of strength and ductility is observed in the nanostructured Al-1.7Fe alloy processed by e-beam deposition [55]. The average sub-grain size of 85 nm was observed in the microstructure of an Al-1.7Fe alloy with an average grain size of 2 μm with high-angle misorientations. Since there is no evidence of Fe-bearing second-phase particles in the Al-1.7Fe alloy, as manifested by only five Al peaks in X-ray diffraction patterns and only Al circles in SAED patterns in TEM observation, it was concluded that the Al-1.7Fe alloy is a supersaturated solid solution. Furthermore, lattice distortions in the nano-scale range were observed in high resolution electron microscopy (HREM), which might be attributed to the possible presence of defects, clusters of the alloy atoms, or nano-scale precipitates in the inter-

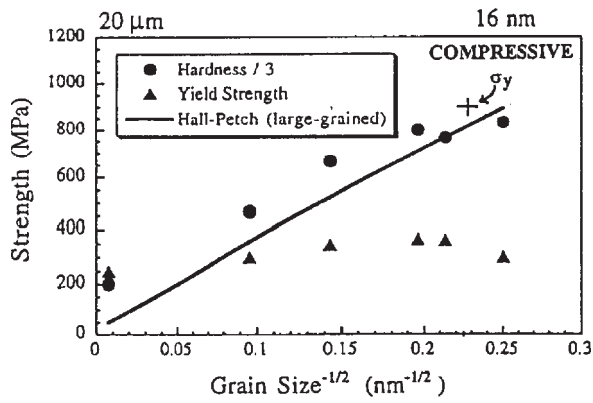
rior of grains. The lattice mismatch and lattice bending in the vicinity of lattice mismatch were also observed in the Al-1.7Fe alloy by HREM. A better strength and ductility balance is considered to arise from the nano-scale grain size and the absence of detectable levels of second-phase particles [55]. The low strain hardening or work softening behavior is observed in the material.

3. DISCUSSION

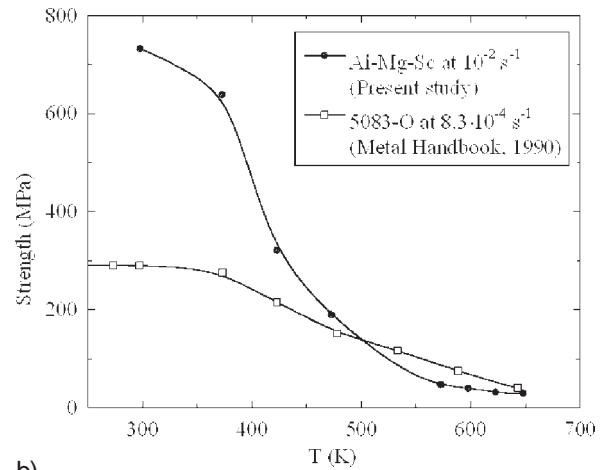
3.1. Effect of processing history on mechanical properties

The aforementioned results indicate that there is a significant effect of processing history on mechanical properties of nanostructured materials. Consolidation of nanostructured materials from milled powders is usually accomplished at lower temperatures in order to avoid significant grain growth. As a result, the possibility of porosity or incomplete bonding usually exists, unless proper processing parameters are selected. Porosity, like the lack of dislocation activity, in nanocrystalline materials is argued to be responsible for poor tensile performance [15,17]. An example in support of this argument can be provided by comparing the tensile yield strength to the compression yield strength in nanocrystalline Cu. For this metal, tensile yield strength, compression yield strength and third of microhardness ($H_v/3$) as a function of (grain size)^{-1/2} for nanocrystalline Cu are shown in Fig. 6a [15]. The values of tensile yield strength are clearly lower than those of compression yield strength and third of microhardness. It is suggested that the asymmetry of yield strength between tension and compression is attributed to the existence of porosity in the consolidated nanostructured materials. A similar asymmetry of yield strength due to the processing defects is also observed in a nanostructured Al-7.5%Mg alloy [32]. In this case, the existence of a few micron-size inclusions in the microstructure is thought to be responsible for the fact that the yield strength and ductility in tension are lower than those in compression.

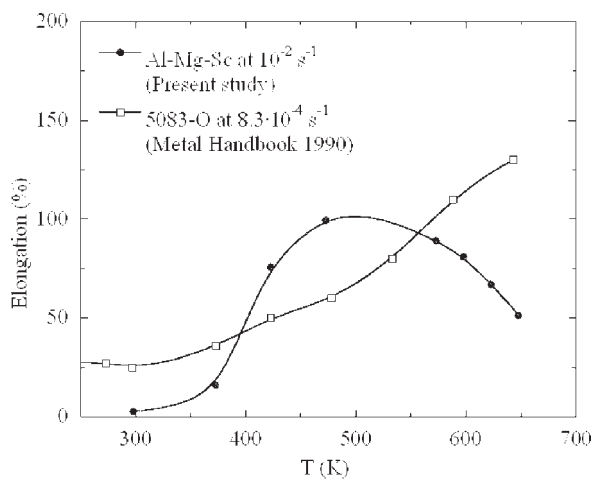
Nanostructured materials processed via consolidation of milled powders usually contain contamination elements and nanoscale dispersoids that are generated during milling. For example, nanostructured Al alloys processed via cryomilling processing usually contain other elements, in addition to their alloying elements [10,29]. Fe, Ni, Cr and Mn were contaminants from the milling media (stainless steel balls and vial) used in the milling



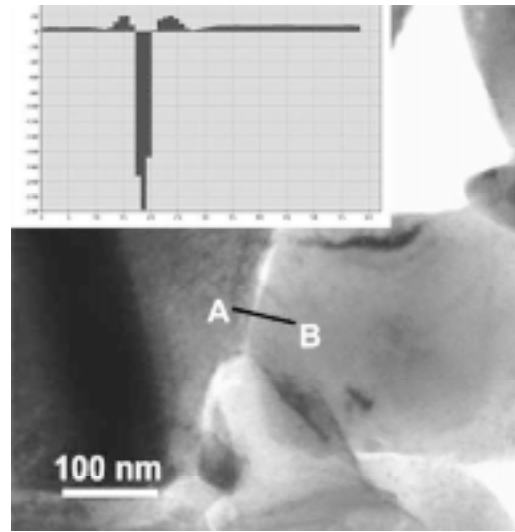
a)



b)



c)



d)

Fig. 6. (a) Tensile yield strength, compression yield strength and $H_v/3$ as a function of $(\text{grain size})^{-1/2}$ for nanocrystalline Cu, taken from [15]; (b) and (c) comparison of mechanical properties of a cryomilled Al-Mg-Sc alloy with conventional 5083 Al [29]; and (d) Segregation of sulfur at grain boundary is evident, taken from [45].

process. N, O, C and H were introduced into the material by a process control agent (0.2 – 0.3 wt. pct of stearic acid $\text{CH}_3(\text{CH}_2)_{16}\text{CO}_2\text{H}$) during cryomilling. In this particular study, Si, Cu, Zn and Ti are thought to have originated from the starting powder materials. The existence of extraneous elements influences both the microstructure and the mechanical performance of the cryomilled Al alloys. Some of the extraneous elements form nanoscale dispersoids during processing, as shown in Fig. 2b. Dislocations and their interactions with nanoscale particles were observed in a few grains. For nanostructured Al alloys processed via cryomilling processing, although porosity can be significantly eliminated by implementing carefully-chosen pro-

cessing routes, contamination cannot be totally avoided, which can have a significant effect on mechanical properties. The segregation of extraneous elements was considered to be one of reasons for the poor mechanical properties at elevated temperatures of a near-nanostructured Al-Mg-Sc alloy, compared to conventional 5083 Al alloy, as shown in Figs. 6b and 6c.

Contamination also exists in processing of nanocrystalline materials by electrodeposition [45]. Segregation of various elements to grain boundaries has a significant effect on mechanical properties of electrodeposited nanocrystalline materials, resulting in the intergranular embrittlement behavior. Although it appears that contamination has a negli-

gible effect on the mechanical properties of the as-deposited nanocrystalline materials, segregation of contamination elements to grain boundaries after annealing will embrittle the material when deformed at room temperature. As shown in Fig. 6d, there is an evidence of segregation of sulfur at grain boundary of nanocrystalline Ni after annealing at a temperature of 523K [45].

3.2. Strain hardening behavior

Based on the Hall-Petch relationship, the strength of nanocrystalline materials increases with decreasing the grain size. It appears that the Hall-Petch relationship in electrodeposited Ni material is kept to a finest grain size of approximately 10 nm [11,56]. Therefore, for most of nanocrystalline materials processed by electrodeposition with grain sizes of 10–40 nm, the dislocation-mediated plasticity plays a dominant role in plastic deformation. A long strain-hardening region after yielding observed in the nanostructured materials processed by electrodeposition could be explained by the theory of dislocation multiplication [57]. The nanostructured materials processed by electrodeposition usually fail after reaching the maximum strength.

In the nanostructured materials processed by milling, a short strain-hardening region after yielding is usually observed. It is interesting to note that although the grain size of nanostructured materials processed by milling is larger than that of nanostructured materials processed by electrodeposition, the strain-hardening region after yielding is shorter in the former material. After the maximum stress, there is an evidence of stress-drop. Similar phenomenon of stress drops is also observed in other MA Al alloys [58-60], in which the stress drop was attributed to the collective movement of large numbers of mobile dislocations that were previously pinned by a complex network of fine dislocation cells. The subsequent flow stress plateau was attributed to the reduced resistance to glide of unpinned dislocations. Since there are small amounts of nanoscale dispersoids in the nanostructured materials processed by milling, the detachment of dislocations from nanoscale oxide or nitride dispersoids is considered to be one possible explanation for the phenomenon of stress-drop. During yielding, dislocations can accumulate around nanoscale dispersoids. When the accumulated dislocations annihilated in the vicinity of nanometric dispersoids under high applied stresses, a stress-drop may occur in the stress-strain curve [34].

In many cases, stress drops in nanostructured materials are associated with the initiation of Lüders bands on the surface of tensile specimens [61]. During Lüders band formation, propagation of the Lüders band is limited by the presence of glide obstacles and does not extend across the gage section of the alloys. Therefore, the deformation strain after the maximum strength in nanostructured materials is mainly related to the formation and propagation of Lüders strain. In the case, ductility of nanostructured materials is attributed to two parts, which consist of the uniform deformation (ϵ_u) and the occurrence of Lüders strain (ϵ_L). The total strain can be expressed as $\epsilon = \epsilon_u + \epsilon_L$.

In previous investigations of Lüders bands in UFG Al-Mg alloys processed via thermomechanical routes [62-65], serrated yielding in the stress-strain curves has been attributed to the interaction of dislocations with Mg solute atoms. Recent investigations of Lüders bands in UFG Al-Mg alloys [66] have revealed that Lüders band formation is influenced not only by Mg solute pinning and grain size, but also by the material processing history and the deformation conditions. In particular, the presence or absence of Lüders effect is related to grain boundary structure. According to one study [66], the Lüders effect is observed when dislocation-free boundaries are formed during processing. Conversely, if a high concentration of grain boundary dislocations is formed during processing, the Lüders effect may be absent.

Following the initiation of Lüders band (in flat dog-bone specimens) or necking (in cylindrical dog-bone specimens), the phenomenon of the low strain hardening or work softening behavior is often observed in the stress-strain curves. This trend is manifested in the presence of a longer steady-stage extending from the ultimate stress to the failure point. A low strain hardening or work softening behavior is another characteristic that is often observed in the tensile deformation of many materials [9,10,29,39,55,58-60,67-69]. In the investigation of MA aluminum alloys, the work softening behavior was explained by the modified theory of low energy dislocation structure (LEDS) [59,70]. It was proposed that the work softening was accomplished through the reduction of dislocation density or the reduction of the Hall-Petch strengthening. It is widely accepted that the strength of crystalline materials in terms of the critical resolved shear stress (τ) on the operative glide systems is correlated with the dislocation density (ρ):

$$\tau = \tau_0 + \alpha Gb\sqrt{\rho}, \quad (2)$$

where τ_0 is the friction stress acting on the dislocation sliding and a equals to 0.4 within a factor of two or so. During straining, the critical shear stress increases with increasing dislocation density. Nevertheless, in nanostructured materials processed via milling, it is quite possible that exceptionally high dislocation densities have been introduced during the course of mechanically milling. For instance, the high dislocation densities of $1.3 \cdot 10^{17} \text{ m}^{-2}$ are observed in the cryomilled Al-Mg powders with a grain size of $\sim 25 \text{ nm}$ [30,71]. After consolidation, the dislocation densities in the cryomilled Al alloys might be still high, since dislocations were clung to the nanoscale dispersoids in the microstructure, which were generated during the milling. Such high dislocation densities might be higher than those under equilibrium conditions. The subsequent plastic deformation will reduce the initial dislocation density and thus the flow stress, since every new glide dislocation loop will give rise to the annihilation of more than its own length, resulting in the work softening [59]. Work softening may also be due to a reduction in the friction stress of the Hall-Petch strengthening as in dislocation unlocking from impurity or alloying atmosphere, or the breaking of barriers in grain or dislocation structures [57].

Another explanation for the low strain hardening or work softening behavior is the occurrence of dynamic recovery during plastic deformation [34,57]. Mobile dislocations can be trapped by both impenetrable obstacles and forest dislocations, forming additional obstacles to glide that contribute to strain hardening. On the other hand, immobile dislocations may annihilate due to cross-slip or rearrange to form sub-boundaries of relatively low energy, contributing to dynamic recovery [72,73]. Dynamic recovery was considered to take place in the low-strain-hardening region of the tensile and compressive behavior of UFG AlFeVSi alloy [74]. Although solute additions usually retard dynamic recovery by increasing lattice frictional stress, inhibiting dislocation slip, a high disorder region as well as the associated high vacancy concentration in cryomilled Al alloys may facilitate recovery, causing low strain hardening and a relatively high ductility.

3.3. Ductility of nanostructured materials

Although the strength increase follows the Hall-Petch relationship in most of the nanostructured materials reviewed in the present paper, a ductility decrease with decreasing grain size is evident, despite considerable scatter in the data [75,76]. The processing approach has an influence on the value

of elongation. For instance, for the same grain size, the values of elongation in nanostructured aluminum alloys by severe plastic deformation are higher than those by consolidation of mechanically milled powders [76]. As reported elsewhere [18,77], the low tensile ductility of many nanostructured materials is often attributed to processing defects and flaws (porosity or poor interfacial bonding). The low ductility in nanostructured materials by milling may also be related to the lower density of mobile dislocations (ρ_m). The value of uniform strain (ϵ_u) can be expressed as:

$$\epsilon_u = \rho_m b L, \quad (3)$$

where b the Burgers vector and L is the average distance of dislocation movement. In nanostructured materials processed via consolidation of mechanically milled powders, most of the dislocations are most likely to be immobilized due to their strong interactions of dislocations with nanoscale dispersoids.

In order to overcome the low ductility problems in nanostructured materials, several bimodal cryomilled Al-Mg alloys are processed with both the same processing routes and the parameters except containing the different volume fractions (15 and 30 wt. pct) of unmilled submicron-grained powders [33]. After consolidation, they were extruded using the same parameters to eliminate the residual porosity and improve mechanical properties. The grain size in the nanostructured regions and in the submicron-grained regions is 100 – 300 nm and 1 μm , respectively [33]. According to previous studies on two-phase cryomilled Al alloys, there is no much change in the microstructure of nanostructured regimes after extrusion [78]. However, there is a directional distribution of submicron-grained regions after extrusion, which is elongated along the extrusion direction [39-41,78].

There is a decrease in strength while ductility increases with increasing fraction of submicron-grained regions in cryomilled nanostructured materials, as shown in Fig. 3b. The observed decrease in yield strength of the bimodal Al alloys with increasing coarse-grain fractions is attributed to the load transfer to softer constituents. The relationship between yield strength ($\sigma_{0.2}$) and volume fraction (V_u) of unmilled powders can be approximated by a simple rule of mixtures,

$$\sigma_{0.2} = (1 - V_u)\sigma_c + V_u\sigma_u, \quad (4)$$

where σ_c and σ_u are the yield stress of nanostructured materials processed with 100 pct cryomilled pow-

ders and 100 pct unmilled powders, respectively. Adding submicron grains into the nanostructured matrix will bring both enhanced dislocation activity as well as longer distance of dislocation movement in the materials, resulting in a higher ductility. Although there is a significant increase in ductility in bimodal cryomilled materials, the duration of strain hardening region (uniform strain) is not increased as expected and a longer low strain hardening behavior (or work softening behavior) is observed.

The microstructure of nanostructured materials with the bimodal grain size distribution processed via powder metallurgy routes is analogous to short-fiber metal matrix composites, in that the submicron-grained bands are distributed parallel to the extrusion direction. The bands tend to be discontinuous when the volume fraction of coarse gains is low, and continuous when the volume fraction of coarse gains is high. Metal matrix composites usually have lower fracture toughness and low ductility than unreinforced matrix materials although they possess higher specific stiffness and strength. Laminated metal composites with ductile layers are developed for the purpose of improvement of the ductility and toughness [79,80]. Several toughening mechanisms have been proposed to explain ductile-phase toughening of composite microstructures, such as crack bridging, crack blunting, crack deflection, stress distribution of crack tip, crack front convolution and local plane stress deformation, *etc.* [79,81].

On the basis of microstructural characteristics of bimodal nanostructured materials, a model of crack blunting combined with the concept of delamination has been developed, as illustrated in Fig. 7 [61]. The figure shows the propagation of a microcrack in a nanostructured material with a bimodal lamellar structure. In the bimodal Al alloys, microcracks are expected to nucleate first in the harder nanostructured regions and propagate along grain boundaries. When a microcrack meets a submicron-grained band, the band will retard propagation by blunting the crack and/or by delamination of interfaces between submicron-grained and nanostructured-grain regions, as shown in Fig. 7a. When more dislocations are emitted into the submicron grain, a new slip surface may be formed, eventually leading to necking and cavitation within the submicron-grained bands, as shown in Fig. 7b. Finally, dimples on the submicron-grained regions and delamination at interfaces will be generated on fracture surface (as revealed in Fig. 7c). The delamination at interfaces and the necking deformation of

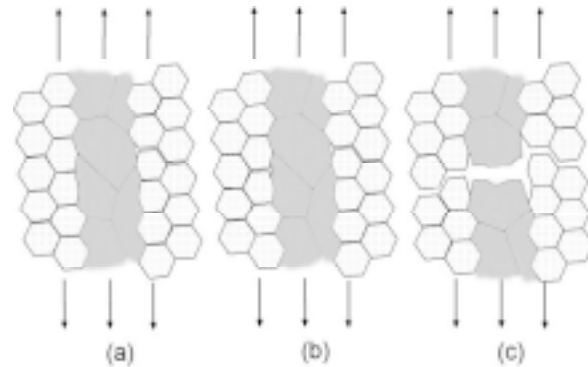


Fig. 7. Delamination and bridging mechanisms in a bimodal microstructure [61].

ductile submicron-grain regions will cause significant energy loss, resulting in an enhanced tensile ductility.

4. SUMMARY AND CONCLUSIONS

The mechanical properties of nanostructured materials processed by consolidation of nanocrystalline powders and by electrodeposition are reviewed. The nanocrystalline materials obtained by consolidation of powder of inert-gas condensation contain processing defects – that have a significant effect on mechanical properties, resulting in low ductility. The nanostructured materials processed by cryomilling have a good combination of strength and ductility. However, because of experiencing several thermo-mechanical routes, grain sizes in cryomilled nanostructured materials usually grow to the range of 100 – 200 nm. A short region of strain hardening, followed by a long region of low strain hardening or work softening behavior is usually observed in the plastic deformation of nanostructured materials processed by milling. The nanostructured materials processed by electrodeposition have a grain size of 10 – 40 nm. Although the grain in nanocrystalline materials processed by electrodeposition is smaller than that by milling, significant strain hardening region is observed in the former materials.

The processing history has a significant effect on mechanical properties of nanostructured materials. Asymmetry of yield strength between tension and compression is attributed either to the existence of porosity or to the bimodal phase distribution. Strain hardening in nanostructured materials can be explained by the theory of dislocation multiplication. The low strain hardening behavior in nanostructured materials processed by milling can

be attributed to dislocation annihilation or dynamic recovery during plastic deformation. Low ductility in nanostructured materials can be overcome by adding submicron grains into nanostructured region for the formation of bimodal microstructures.

ACKNOWLEDGEMENTS

The work was supported in part by the National Science Foundation (Grant number DMR-0304629) and in part by the Office of Naval Research with Dr. Lawrence Kabacoff as program officer (Grant number N00014-03-1-0149).

REFERENCES

- [1] C. Suryanarayana // *Inter. Mater. Rev.* **40** (1995) 41.
- [2] W. W. Milligan, In: *Comprehensive structural integrity*, ed. by I. Milne, R. O. Ritchie, and B. Karihaloo (Elsevier Pergamon, 2003, Vol. 8) p. 529.
- [3] *Nanostructured Materials: Processing, Properties and Potential Applications*, ed. by C. C. Koch (Noyes Publications, William Andrew Publishing, Norwich, NY, 2002).
- [4] H. Gleiter // *Prog. Mat. Sci.* **33** (1989) 223.
- [5] A. M. Elsharik and U. Erb // *J. Mater. Sci.* **30** (1995) 5743.
- [6] R. Birringer // *Mat. Sci. Eng. A* **117** (1989) 33.
- [7] K. Lu // *Mat. Sci. Eng.* **R16** (1996) 161.
- [8] R. Z. Valiev, R. K. Islamgaliev and I. V. Alexandrov // *Prog. Mat. Sci.* **45** (2000) 103.
- [9] X. K. Sun, H. T. Cong, M. Sun and M. C. Yang // *Metall. Mater. Trans. A* **31A** (2000) 1017.
- [10] V. L. Tellkamp, A. Melmed and E. J. Lavernia // *Metall. Mater. Trans. A* **32A** (2001) 2335.
- [11] F. Ebrahimi, G. R. Bourne, M. S. Kelly and T. E. Matthews // *NanoStruct. Mater.* **11** (1999) 343.
- [12] F. A. Mohamed and Y. Li // *Mat. Sci. Eng. A* **298** (2001) 1.
- [13] M. N. Rittner, J. R. Weertman and J. A. Eastman // *Acta Mater.* **44** (1996) 1271.
- [14] P. G. Sanders, G. E. Fougere, L. J. Thompson, J. A. Eastman and J. R. Weertman // *NanoStruct. Mater.* **8** (1997) 243.
- [15] P. G. Sanders, J. A. Eastman and J. R. Weertman // *Acta Mater.* **45** (1997) 4019.
- [16] G. W. Nieman, J. R. Weertman and R. W. Siegel // *J. Mater. Res.* **6** (1991) 1012.
- [17] C. J. Youngdahl, P. G. Sanders, J. A. Eastman and J. R. Weertman // *Scripta Mater.* **37** (1997) 1997.
- [18] M. N. Rittner, J. R. Weertman, J. A. Eastman, K. B. Yoder and D. S. Stone // *Mat. Sci. Eng. A* **237** (1997) 185.
- [19] H. J. Fecht // *NanoStruct. Mater.* **6** (1995) 33.
- [20] J. Eckert, J. C. Holzer, I. C.E. Krill and W. L. Johnson // *J. Mater. Res.* **7** (1992) 1751.
- [21] C. C. Koch // *NanoStruct. Mater.* **9** (1997) 13.
- [22] F. A. Mohamed // *Acta Mater.* **51** (2003) 4107.
- [23] J. E. Carsley, A. Fisher, W. W. Milligan and E. C. Aifantis // *Metall. Mater. Trans. A* **29A** (1998) 2261.
- [24] J. R. Ryu, K. I. Moon and K. S. Lee // *J. Alloys & Comp.* **296** (2000) 157.
- [25] Q. Wei, T. Jiao, K. T. Ramesh and E. Ma // *Scripta Mater.* **50** (2004) 359.
- [26] Y. Champion, C. Langlois, S. Guerin-Mailly, P. Langlois, J.-L. Bonnentien and M. J. Hytch // *Science* **300** (2003) 310.
- [27] D. Jia, Y. M. Wang, K. T. Ramesh, E. Ma, Y. T. Zhu and R. Z. Valiev // *Appl. Phys. Lett.* **79** (2001) 611.
- [28] Q. Wei, D. Jia, K. T. Ramesh and E. Ma // *App. Phys. Lett.* **81** (2002) 1240.
- [29] B. Q. Han, E. J. Lavernia and F. A. Mohamed // *Metall. Mater. Trans. A* **36A** (2005) 345.
- [30] F. Zhou, X. Z. Liao, Y. T. Zhu, S. Dallek and E. J. Lavernia // *Acta Mater.* **51** (2003) 2777.
- [31] F. Zhou, S. R. Nutt, C. C. Bampton and E. J. Lavernia // *Metall. Mater. Trans. A* **34A** (2003) 1985.
- [32] B. Q. Han, F. A. Mohamed, C. C. Bampton and E. J. Lavernia, In: *MRS Proc. 2004*, Q1.7.1-6.
- [33] D. Witkin, Z. Lee, R. Rodriguez, S. Nutt and E. Lavernia // *Scripta Mater.* **49** (2003) 297.
- [34] B. Q. Han, Z. Lee, S. R. Nutt, E. J. Lavernia and F. A. Mohamed // *Metall. Mater. Trans. A* **34A** (2003) 603.
- [35] E. M. Taleff, D. R. Lesuer and J. Wadsworth // *Metall. Mater. Trans. A* **27A** (1996) 343.
- [36] R. Q. Ye, B. Q. Han and E. J. Lavernia // *Metall. Mater. Trans. A* (2004), submitted.
- [37] E.V.D. Giessen and A. Needleman // *Annu. Rev. Mater. Res.* **32** (2002) 141.
- [38] S. Schmauder // *Annu. Rev. Mater. Res.* **32** (2002) 437.
- [39] R. W. Hayes, R. Rodriguez and E. J. Lavernia // *Acta Mater.* **49** (2001) 4055.
- [40] Z. Lee, R. Rodriguez, R. W. Hayes, E. J. Lavernia and S. R. Nutt // *Metall. Mater. Trans. A* **34A** (2003) 1473.

- [41] B. Q. Han, E. J. Lavernia and F. A. Mohamed // *Mat. Sci. Eng. A* **358** (2003) 318.
- [42] U. Erb // *NanoStruct. Mater.* **6** (1995) 533.
- [43] W. M. Yin, S. H. Whang, R. Mirshams and C. H. Xiao // *Mater. Sci. Eng. A* **301** (2001) 18.
- [44] F. D. Torre, H. V. Swygenhoven and M. Victoria // *Acta Mater.* **50** (2002) 3957.
- [45] Y. M. Wang, S. Cheng, Q. M. Wei, E. Ma, T. G. Nieh and A. Hamza // *Scri. mater.* **51** (2004) 1023.
- [46] A. Hasnaoui, H. V. Swygenhoven and P. M. Derlet // *Acta Mater.* **50** (2002) 3927.
- [47] Y. M. Wang and E. Ma // *App. Phys. Lett.* **85** (2004) 2750.
- [48] H. Iwasaki, K. Higashi and T. G. Nieh // *Scri. mater.* **50** (2004) 395.
- [49] A. F. Zimmerman, G. Palumbo, K. T. Aust and U. Erb // *Mat. Sci. Eng. A* **328** (2002) 137.
- [50] L. Lu, S. X. Li and K. Lu // *Scri. mater.* **45** (2001) 1163.
- [51] L. Lu, L. B. Wang, B. Z. Ding and K. Lu // *J. Mater. Res.* **15** (2000) 270.
- [52] L. Lu, M. L. Sui and K. Lu // *Science* **287** (2000) 1463.
- [53] A.A. Karimpoor, U. Erb, K.T. Aust and G. Palumbo // *Scri. mater.* **49** (2003) 651.
- [54] H. Sasaki, K. Kita, J. Nagahora and A. Inoue // *Mater. Trans.* **42** (2001) 1561.
- [55] T. Mukai, S. Suresh, K. Kita, H. Sasaki, N. Kobayashi, K. Higashi and A. Inoue // *Acta Mater.* **51** (2003) 4197.
- [56] G. D. Hughes, S. D. Smith, C. S. Pande, H. R. Johnson and R. W. Armstrong // *Scri. metall.* **20** (1986) 93.
- [57] D. Kuhlmann-Wilsdorf // *Phil. Mag. A* **79** (1999) 955.
- [58] Y. W. Kim and L. R. Bidwell // *Scri. metall.* **16** (1982) 799.
- [59] H. G. F. Wilsdorf and D. Kuhlmann-Wilsdorf // *Mat. Sci. Eng. A* **164** (1993) 1.
- [60] H. R. Last and R. K. Garrett // *Metall. Mater. Trans. A* **27A** (1996) 737.
- [61] B. Q. Han, Z. Lee, D. Witkin, S. R. Nutt and E. J. Lavernia // *Metall. Mater. Trans. A* (2005), in print.
- [62] D. J. Lloyd and L. R. Morris // *Acta Metall.* **25** (1977) 857.
- [63] D. J. Lloyd // *Met. Sci. May* (1980) 193.
- [64] D. J. Lloyd // *Metall. Trans. A* **11A** (1980) 1287.
- [65] T. Mukai, K. Ishikawa and K. Higashi // *Mater. Sci. Eng. A* **204** (1995) 12.
- [66] D. J. Lloyd, S. A. Court and K. M. Gatenby // *Mat. Sci. Tech.* **13** (1997) 660.
- [67] T. Mukai, M. Kawazoe and K. Higashi // *NanoStruct. Mater.* **10** (1998) 755.
- [68] S. Y. Chang, J. G. Lee, K. T. Park and D. H. Shin // *Mat. Trans.* **42** (2001) 1074.
- [69] T. Hasegawa, T. Miura, T. Takahashi and T. Yakou // *ISIJ Int.* **32** (1992) 902.
- [70] D. Kuhlmann-Wilsdorf and H. G. F. Wilsdorf // *phys. stat. sol. (a)* **172** (1992) 235.
- [71] X. Z. Liao, J. Y. Huang, Y. T. Zhu, F. Zhou and E. J. Lavernia // *Phil. Mag. A* **83** (2003) 3065.
- [72] R. Kral // *phys. stat. sol. (a)* **157** (1996) 255.
- [73] F. J. Humphreys and M. Hatherly, *Recrystallization and Related Annealing Phenomena* (Pergamon, New York, 1995).
- [74] S. Hariprasad, S. M. L. Sastry and K. L. Jerina // *Acta Mater.* **44** (1996) 383.
- [75] C. C. Koch, D. G. Morris, K. Lu and A. Inoue // *MRS Bulletin Feb.* (1999) 54.
- [76] B. Q. Han, F. A. Mohamed and E. J. Lavernia // *J. Mater. Sci.* **38** (2003) 3319.
- [77] J. R. Weertman // *Mater. Sci. Eng. A* **166** (1993) 161.
- [78] Z. Lee, R. Rodriguez, E. J. Lavernia and S. R. Nutt, In: *Ultrafine Grained Materials II*, ed. by Y.T. Zhu *et al.* (TMS, 2002), p. 653.
- [79] D.R. Lesuer, C.K. Syn, O.D. Sherby, J. Wadsworth, J.J. Lewandowski and W.H. Hunt, Jr. // *J. Inter. Mater. Rev.* **41** (1996) 169.
- [80] A.B. Pandey, B.S. Majumdar and D.B. Miracle // *Acta mater.* **49** (2001) 405.
- [81] W. Soboyejo, *Mechanical properties of engineered materials* (Marcel Dekker, Inc., New York, 2003).